Computational Materials Science 240 (2024) 113013

Contents lists available at ScienceDirect

Computational Materials Science

journal homepage: www.elsevier.com/locate/commatsci

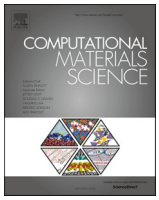

Full Length Article

Improved carbide volume fraction estimation in as-cast HCCI alloys using machine learning techniques

U. Pranav Nayak [a,1,*], Martin Müller [a,b,1], Noah Quartz [a], M. Agustina Guitar [a], Frank Mücklich [a,b]

[a] Department of Materials Science, Saarland University, Campus D3.3, D-66123 Saarbrücken, Germany
[b] Material Engineering Center Saarland (MECS), Campus D3.3, D-66123 Saarbrücken, Germany

ARTICLE INFO

Keywords:
Carbide volume fraction
High chromium cast iron
Machine learning
Metallography
Microstructure
Phase quantification

ABSTRACT

An improved approach is presented for the estimation of carbide volume fraction (CVF) in as-cast High Chromium Cast Iron (HCCI) alloys using Machine Learning (ML) techniques. The limitations of existing formulae for CVF estimation in HCCI alloys, which relied on a limited number of alloy compositions, are addressed. A comprehensive dataset comprising 320 distinct alloy compositions from 60 different sources was compiled. ML models trained on this dataset revealed the significant influence of carbon (C), chromium (Cr), and molybdenum (Mo) on CVF determination. By leveraging ML algorithms, a predictive model was developed that offers enhanced accuracy in estimating CVF across a wider range of compositions. This ML-based approach provides researchers with a valuable tool for determining CVF in as-cast HCCI alloys, minimizing the need for resource-intensive and time-consuming experimental procedures. The results obtained demonstrate improved CVF estimation accuracy and broader applicability, thus facilitating more efficient and reliable CVF determination in HCCI alloys.

1. Introduction

High chromium cast irons (HCCIs) are a subset of abrasion-resistant white cast irons (WCIs), offering superior wear resistance and toughness within the WCI category [1,2]. These alloys, based on the Fe-Cr-C ternary system, typically contain 11–30 wt% chromium (Cr) and 2–4 wt% carbon (C) according to ASTM A532 standards [3], along with minor additions of molybdenum (Mo), nickel (Ni), copper (Cu), and manganese (Mn) [4]. Characterized by hard eutectic carbides (EC) dispersed in a modifiable matrix (austenite, ferrite, martensite), HCCIs can possess up to 50 % carbides by volume due to their wide compositional range [5–8]. The carbides exhibit a hardness range of 1200–1600 HV [9,10], contributing synergistically with the matrix to enhance both wear resistance and toughness. These properties make HCCIs suitable for various industrial applications, including ore crushers, ball mill liners, and grinding equipment [4,11,12].

Extensive research has been conducted by numerous researchers to identify the optimal carbide volume fraction (CVF) for enhancing hardness and wear resistance, with some studies maintaining the matrix microstructure relatively unchanged [13–19]. However, an increase in hardness does not necessarily correlate with improved wear resistance [20]. Zum Gahr et al. [21] and Doğan et al. [22] observed increased material hardness with higher CVF, but without a commensurate improvement in wear resistance. Notably, Doğan et al. [22] noted a significant reduction in wear volume loss for a 26 wt% Cr WCI with an austenitic matrix and a CVF of 28 % compared to a 16 wt% Cr WCI with a pearlitic/bainitic matrix and a CVF of 45 %.

Moreover, in low-stress abrasion scenarios, where the abrasive was softer than the carbides but harder than the matrix, increasing CVF improved wear resistance [19,21,23]. Conversely, under high-stress or three-body abrasion, microcracking of carbide tips occurred, indicating a threshold beyond which further increases in CVF became detrimental to wear resistance [4,21,24]. However, accurately predicting the CVF in as-cast HCCI alloys is a complex task due to the intricate nature of carbide formation and the influence of various alloying elements.

Over the years, researchers have employed experimental approaches

* Corresponding author.
E-mail addresses: pranav.nayak@uni-saarland.de (U.P. Nayak), martin.mueller1@uni-saarland.de (M. Müller), noah.quartz@uni-saarland.de (N. Quartz), a.guitar@mx.uni-saarland.de (M.A. Guitar), muecke@matsci.uni-sb.de (F. Mücklich).
[1] U.P.N. and M.M. contributed equally to this work.

https://doi.org/10.1016/j.commatsci.2024.113013
Received 15 February 2024; Received in revised form 20 March 2024; Accepted 5 April 2024
Available online 10 April 2024

to estimate CVF in HCCI alloys. Initially, based on metallographic assessments of experimental alloy melts, Maratray and Usseglio-Nanot established a linear relationship between C, Cr and CVF in 1970 [25,26]. The equation was deduced from their study of over 40 different alloys with varying C (1.95–4.31 wt%) and Cr (10.8–25.82 wt%) contents, encompassing Cr/C ratios between 3.5 and 10.2. The CVF was determined through the linear intercept method, with carbides counted in a representative specimen using slices taken from different sections of an ingot. The equation, featured as Equation #1 (M) in Table 1, stands as the prevalent mathematical model for computing CVF in HCCIs and have been implemented in various studies [1,27–30].

In a manner reminiscent of Maratray's approach, Doğan et al. in 1997 formulated an equation establishing a linear relationship between C, Cr, and CVF [22]. Their work focused on hypoeutectic, eutectic, and hypereutectic cast iron compositions, encompassing Cr contents of 15 and 26 wt%. The determination of CVF in the castings was conducted through both wet chemistry and image analysis, yielding comparable results. The resulting equation #2 (D), derived from the analysis presented in Table 1, demonstrates that CVF increases with rising carbon content and experiences a slower increase with higher Cr content. Despite similarities to the equation established by Maratray and Usseglio-Nanot for up to 4 wt% Mo-containing high Cr WCIs,

Equation #2 (D) estimates a slightly lower carbide volume fraction than its counterpart. However, these simplistic formulae had limitations as they were based on a limited number of alloy compositions and exhibited linear relationships.

Chung's investigation comprised of 53 diverse HCCI alloys, ranging in C concentrations from 1 to 6 wt% and Cr concentrations from 5 to 45 wt% [31]. The analyses highlighted carbon's predominant influence in controlling carbide volume fractions, with an increase in carbon content leading to a substantial rise from approximately 15 to 66 %, while a parallel increase in overall chromium concentration resulted in a more modest average increment of 17 % in carbide volume. The work involved surface fitting and comparison with Maratray's empirical equation, revealing that a second-grade polygonal fitting offered a superior adjustment. The proposed empirical equation is presented as Equation #3 (C) in Table 1. Notably, the predictive accuracy of the proposed equation remained robust, particularly for carbide volume contents below 40 %, with deviations increasing somewhat at higher volume fractions of carbides.

Chung, Maratray, and Doğan employed distinct mathematical approaches in formulating their respective equations for predicting CVF.

Table 1
Literature available models with their CVF formulas along with the assigned nomenclature for this work. The elemental input is weight percent unless otherwise mentioned.

Equation No.	Model/Year	Nomenclature	CVF Formula ($\%CVF =$)
1	Maratray et al., [25]/1970	M	$\%CVF = 12.33C + 0.55Cr - 15.2$
2	Doğan et al., [22]/1997	D	$\%CVF = 14.05C + 0.43Cr - 22$
3	Chung [31]/2014	C	$\%CVF = -13.5 + 15.32C + 0.1Cr + 0.08C^2 + 0.02Cr^2 - 0.23(C^*Cr)$
4	Gates Modification [34]/2018	G	$\%CVF = 12.33C + 0.55Cr + 0.298(Mo - 1.25) - 15.2$
5	Pourasiabi Multiple Linear Regression [35]/2022	MLR	$\%CVF = 12.52C + 0.54Cr + 1.06Mo - 17.11$
6	Pourasiabi Multiple Non Linear Regression [35]/2022	MNLR	$\%CVF = 9.485C - 0.04Cr - 3.637Mo + 0.132(C^*Cr) + 0.479(C^*Mo) + 0.159(Cr^*Mo) - 4.371$

While Maratray and Doğan adhered to a linear relationship, Chung introduced a quadratic form. This quadratic equation adds a layer of complexity, allowing for a more detailed representation of the non-linear interactions between C and Cr, and their influence on CVF. Notably, a commonality in the formulations of Maratray, Doğan, and Chung's models is the exclusion of Mo from their equations. Despite the acknowledged influence of Mo on CVF, as recognized in Maratray's alloys and the study by Chung, neither model incorporates Mo in its mathematical expression. Mo, recognized as a moderately strong carbide former comparable to Cr, is believed to partition into carbides [30,32,33].

To overcome the limitation of neglecting Mo in Maratray's equation, Gates et al. introduced a "chromium equivalent" (CrE) (Equation #4 in Table 1; G) [34]. This pragmatic approach involved using CrE instead of Cr in Maratray's formula, defined as Cr + [(Mo − 1.25) × (molecular weight of Cr/molecular weight of Mo)]. Subsequently, advancements in computing power allowed researchers to explore more sophisticated techniques such as multiple regression analysis, incorporating additional elements such as Mo [35]. The statistical analyses conducted by Pourasiabi et al., involving stepwise regression and P-value tests on Maratray's original dataset, confirmed Mo's significance as a predictor, demanding a more explicit evaluation [35]. They addressed this gap by integrating the original alloy compositions from Maratray's work, involving 40 different alloys, into their investigation and developed both a multiple linear regression (MLR) model (Equation #5 in Table 1; MLR) and a multiple non-linear regression (MNLR) model (Equation #6 in Table 1; MNLR). The results revealed that the MNLR model, accounting for independent and first-order interaction effects of various alloying elements, exhibited the best statistical measures, demonstrating superior goodness of fit, compared to the other models.

With the recent advancements in Artificial Intelligence (AI) and Machine Learning (ML), it has become increasingly apparent that implementing these techniques could offer significant improvements in CVF estimation for as-cast HCCI alloys. Following the lead of fields like autonomous driving [36] and biomedicine [37], which adopted AI and ML techniques early on and drove their development, these methods have gained traction in materials science and engineering in recent years. The various fields of application, in which ML facilitated new and improved approaches include, amongst others, discovery and design of new materials [38], microstructure characterization [39–41], property predictions [42], or surrogate modeling [43]. In general, the importance of ML is that it makes problems accessible to automatic processing by computers for which full mathematical modeling is hopeless. Among the benefits of ML are the discovery of structures and hidden patterns in data, and the modeling of unknown, non-linear relationships. In this context ML can be used when conventional modeling approaches, e.g., metallurgical, or thermodynamic modeling, reach their limits or are not accurate enough. This can be process-property correlations or predictions of mechanical or physical properties or of microstructural characteristics. Examples include the prediction of the hardness of maraging steels that achieves better accuracy with metallurgical modeling [44], the prediction of Curie temperature for certain ferroelectric compounds [45] or the approximation of phase diagrams for ternary alloys [46].

The limitations of the existing CVF prediction formulae, their narrow applicability, and the desire for enhanced accuracy across a wider range of compositions have led to the exploration of ML-based approaches. By harnessing the power of ML algorithms, it is possible to analyze large datasets, identify complex relationships between alloy composition and CVF, and develop predictive models that outperform traditional empirical formulae. The objective of this research is to employ ML techniques to improve the determination of CVF in as-cast HCCI alloys, thereby providing a reliable and accessible method for researchers in the field.

A comprehensive dataset comprising 320 alloy compositions from diverse sources was compiled in this study. The dataset spans a broad

spectrum of alloy compositions, with carbon concentrations ranging from 1.38 wt% to 5.5 wt%, chromium concentrations ranging from 5 wt % to 37 wt%, corresponding to Cr/C ratios ranging from 1 to 17. The newly developed ML model was employed for predicting CVF and additionally, a rigorous evaluation of existing models was conducted. By subjecting this extensive dataset to both our ML model and established literature models, we aim to scrutinize their predictive accuracy and identify the most robust model for estimating CVF.

2. Materials and methodology

Fig. 1 represents a schematic overview of the applied workflow. The comprehensive dataset compiled from literature data is split into a training and a test set. A ML regression model for predicting CVF is trained using the training set. This model is evaluated with regard to the test data, the importance of the features and is benchmarked against existing literature formulas for calculating CVF.

2.1. Data compilation from literature

A dataset comprising 320 unique HCCI alloys was compiled from a diverse set of almost 60 sources, including manuscripts and theses. The comprehensive list of references for the compiled dataset is available separately in the Zenodo repository [47]. The dataset included the reported bulk chemical composition from each source and specifically considered CVF values determined through metallography. Notably, CVF values obtained through alternative methods, such as XRD or simulations, were intentionally excluded. The information was organized into an Excel file, offering a breakdown of the chemical composition for each alloy and the metallographically determined CVF, alongside its respective source. The Excel file can also be found in the Zenodo repository [47].

The elemental distribution among the 320 alloys is visually presented in Fig. 2. The bar graph illustrates the count of each element, with the ordinate indicating the frequency and the abscissa representing the individual elements. In line with expectations for HCCI alloys, iron (Fe), carbon (C), and chromium (Cr) are present in 100 % of the alloy compositions. Meanwhile, silicon (Si), manganese (Mn), and molybdenum (Mo) are found in approximately 70 % of the alloys. Nickel (Ni) is present in about 50 % of the alloys, whereas the presence of copper (Cu) and niobium (Nb) falls below 25 %. Elements tungsten (W), vanadium (V), titanium (Ti), and boron (B) make up smaller fractions, appearing in approximately 6 %, 4 %, and 2 % of the alloys, respectively.

2.2. Literature available models

In the exploration of HCCI alloys, six available models predicting CVF using diverse methodologies were identified in the literature. Maratray and Usseglio-Nanot's foundational linear equation (Equation #1) initiated this exploration, followed by Doğan's work with a similar linear framework (Equation #2). Chung introduced quadratic elements to capture non-linear interactions between C and Cr (Equation #3). Addressing the oversight of Mo in Maratray's equation, Gates proposed a 'chromium equivalent' (CrE) (Equation #4). Pourasiabi et al. further refined the understanding, explicitly considering Mo and introducing both multiple linear regression (MLR) and multiple non-linear regression (MNLR) models in their study (Equations #5 and #6). Table 1 provides a brief overview of the CVF prediction formulas, along with the assigned nomenclature for each model. The elemental input is weight percent unless otherwise mentioned.

The alloy compositions' C, Cr, and, where applicable, Mo content served as inputs for each model. For every alloy composition in the dataset, the experimental CVF was compared with the values obtained from each literature model, and the corresponding deviation (%) was calculated.

2.3. Machine learning approaches

Since not every literature source specifies every alloying element, values of missing elements are set to zero. Besides data standardization no other data preprocessing was performed. The dataset was randomly split into a training set (80 %) and a test set (20 %). Training of the ML regression models was done in MATLAB regression learner app (Version R2023a).

During tests for finding the optimal model parameters, 5-fold cross-validation was used. Firstly, various typical ML algorithms were tested in preliminary trials (e.g., decision tree, random forest, support vector machine, artificial neural network). Ultimately, a Gaussian Process Regression (GPR) model with an exponential kernel performed best. Additionally, it gives the benefit of a probabilistic approach to prediction by giving the mean and standard deviation as output when predicting. Secondly, a feature reduction was carried out. For higher confidence in the feature selection, three feature ranking algorithms were combined: F-Test, Minimum Redundancy Maximum Relevance (MRMR) algorithm, and RReliefF algorithm. For each feature (i.e., chemical element) scores from all three rankings were normalized between 0 and 1 and then an average score was calculated. Based on this average score, the final feature ranking was performed. An iterative manual feature elimination down to two chemical elements was carried out and was then matched against the metallurgical domain expertise. For the final model a hyperparameter optimization was performed (Bayesian optimization with 200 iterations in MATLAB regression learner app).

The metrics mean absolute error (MAE), root mean squared error (RMSE) and coefficient of determination (R^2) are used to evaluate the regression models. The reported models are evaluated on the held-out test set. After determining the optimal parameters, the final model was trained with the entire data set for its series application. For a sufficiently large sample, the benchmark against existing literature formulae for determining the CVF was also performed on the entire data set.

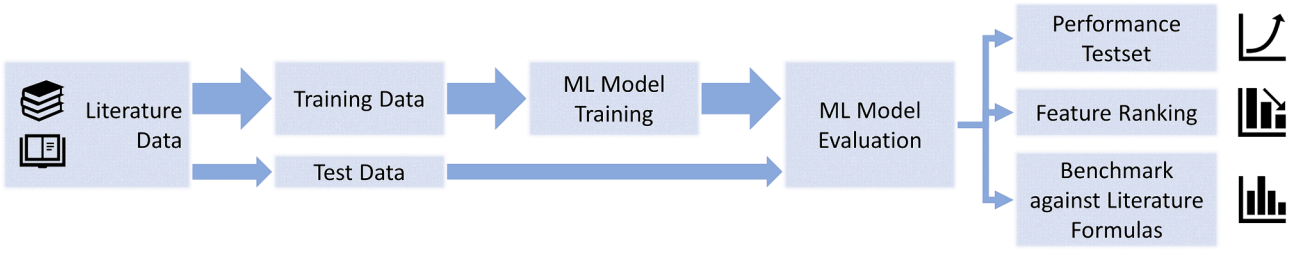

Fig. 1. Schematic overview of the process flow: the data compiled from literature is split into training and test data – after training the model, its evaluation yields the performance on the test set, a feature ranking, and a benchmark against existing formulas from the literature.

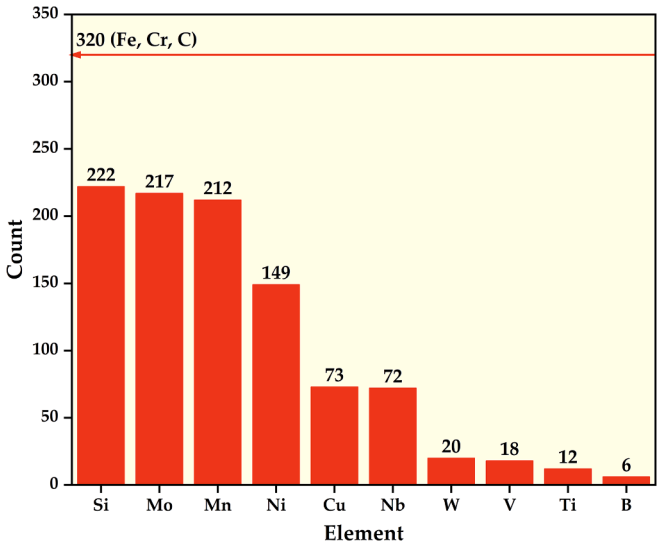

Fig. 2. Elemental count of the 320 HCCI alloys considered in this work.

3. Results and discussion

3.1. Model development and selection

The first model with all 11 elements as input (GPR with exponential kernel, beta = 44.3484, sigma = 1.8454, other model parameters set to default according to MATLAB regression learner app) reaches a MAE of 2.40 %, a RMSE of 3.71 % and a R^2 of 0.896. Generally speaking, a simpler ML model with fewer but relevant features promises better generalization [48]. Table 2 shows the cumulative feature ranking, while Fig. 3 shows the performance of the separate models after the iterative feature elimination. The feature ranking agrees with the domain expertise, i.e., the metallurgical point of view, as the top three elements C, Cr, Mo coincide with the consensus on the important carbide forming elements in HCCI [1,4,31,49,50].

The interplay between the number of features and model performance is illustrated in Fig. 3. This graph showcases how MAE, RMSE, and R2 vary across different features, providing insights into the model's sensitivity. By reducing the number of features, first a decrease in model performance can be noticed (decrease of R2, increase of MAE and RMSE). However, by further reducing the number of features, the performance improves again and keeps a similar level as the first model with all features. Indeed, the lowest values of MAE and RMSE are achieved for the model with only three features. Only by reducing the number of features to only two elements (C, Cr) the performance drops again.

Therefore, the three features C, Cr, and Mo are considered for the final model, as the performance closely aligns with the performance of the comprehensive 11-feature model, but the simpler model promises a better generalization on new data during serial application. To summarize, Fig. 3 offers a visual understanding of the model's adaptability to varying features, emphasizing the practical benefits of a streamlined, three-feature model for optimal predictive accuracy. The three-feature model also reflects the metallurgical domain knowledge. This involves the fact that some elements such as Ni, Cu, Mn etc., have a negligible influence on carbide formation [1,4,51] as well as that the two elements C and Cr alone don't have enough predictive power [34,35].

A hyperparameter optimization (Bayesian optimization with 200 iterations) did not yield a performance improvement compared to the default settings of the initial GPR model in the MATLAB Regression Learner App. Table 3 highlights the efficiency of the final, three-feature model with an MAE of 2.44 %, RMSE of 3.56 %, and an R^2 of 0.905.

For a serial application as well as the benchmarking against existing literature formulas, the final model was trained using the entire data set and the three features (C, Cr, Mo) with the GPR hyperparameters specified in Table 4.

Table 2
Cumulative feature ranking of chemical elements.

Cumulative Feature Rank	Feature	Cumulative Score
1	C	1.00
2	Cr	0.32
3	Mo	0.27
4	V	0.24
5	Nb	0.20
6	W	0.17
7	Cu	0.16
8	Ti	0.14
9	Ni	0.13
10	Si	0.13
11	Mn	0.08

3.2. Model evaluation

To compare our developed ML model with existing literature formulas, CVF for the entire dataset has been calculated according to all literature formulas, and performance metrics have been assessed. In Fig. 4, the performance of all existing literature formulas and our ML model is depicted, emphasizing MAE, RMSE, and R^2 values. An interesting observation emerges when considering the MLR and MNLR models. Their respective MAE, RMSE and R^2 values demonstrate notable similarities. This consistency between the MLR and MNLR models suggests a robustness in predictive performance, highlighting a stable predictive framework across these two regression approaches. Notably, the

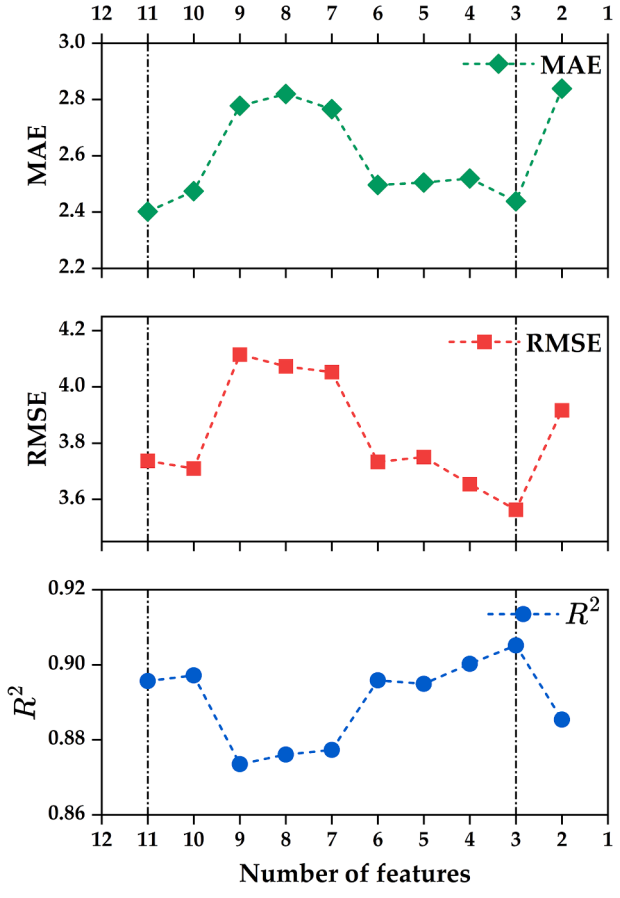

Fig. 3. Variation in model performance with different feature combinations.

Table 3
Comparison of model metrics (MAE, RMSE and R^2) with 11 and 3 features.

Model	MAE [%]	RMSE [%]	R^2 [-]
Initial model with all features	2.40	3.71	0.896
Final optimized model with 3 features	2.44	3.56	0.905

Table 4
Hyperparameters of final GPR model with 3 features.

Basis function	Kernel function	Kernel parameters	Beta	Sigma
Constant	Exponential	84.51, 34.14	49.49	3.91

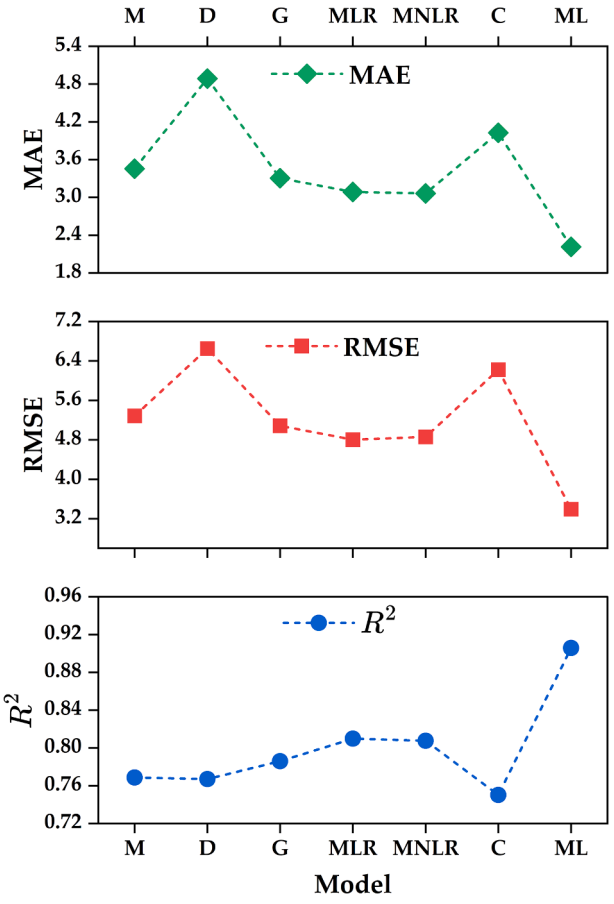

Fig. 4. MAE, RMSE and R^2 values for all models.

lowest MAE and RMSE values are observed in our ML model, emphasizing its superior accuracy. A substantial R^2 value of 0.91 is achieved by the ML model, affirming its reliability in predicting CVF when compared to other models (see Fig. 4).

The distribution plot (Fig. 5a), featuring the ML model as a solid black line and other models as dotted lines, delineates the absolute deviation (%) against the relative frequency, with an inset focusing on values up to 5 % deviation. The peak of the ML model's distribution curve (essentially the mode), closer to zero, indicates a higher concentration of alloys with lower deviations. As deviation increases, the steepest reduction in relative frequency is observed with the ML model, emphasizing its capability to yield fewer alloys with higher deviations. This trend is better visualized with the rug plot, where a notable concentration of alloys for lower deviations for the ML model (black bars) compared to the rest.

Complementing this, the cumulative distribution plot (Fig. 5b), inclusive of an inset capturing values up to 20 %, reveals that at a 20 % deviation threshold, 95 % of alloys fall within this range for the ML model, compared to 85 % for the MNLR model and approximately 70 % for the M model. Notably, at a 10 % deviation threshold, around 80 %, 70 %, and 45 % of alloys fall under this range for the ML, MNLR, and M models, respectively. The combined insights from the distribution rug plot and cumulative distribution plot offers a comprehensive view of the precision of CVF predictions and underscores the value of integrating these graphical representations to gain a more holistic understanding of the predictive performance of ML models in materials characterization.

The scatter box plot analysis depicted in Fig. 6 vividly illustrates the deviations observed across different models for all the alloys. Notably, the ML model emerges with the least spread, indicating a more concentrated and reliable predictive performance. Moreover, the inset table in the graph indicates that the absolute median deviation is the least for the ML model at 4.67 %, highlighting its consistent accuracy, especially in handling diverse datasets. The absolute median deviation serves as a robust metric, providing insight into the central tendency of the model's predictive performance, particularly beneficial when considering a diverse dataset. Furthermore, comparing this metric, which excludes outliers, with the MAE, adds depth to the evaluation, reinforcing the ML model's predictive accuracy.

As mentioned earlier, in this study, we broadened the chemical composition range, resulting in a Cr/C ratio spanning 1 to 17. In comparison, Maratray's original model focused on a narrower range of C and Cr, with Cr/C ratios ranging from 3.5 to 10. This expansion enriched the dataset, allowing for a comprehensive evaluation of the various models' predictive capabilities across a wider alloy composition spectrum, capturing variations in C, Cr and Cr/C ratios more thoroughly.

The heatmap in Fig. 7 illustrates the distribution of alloy counts across various deviation ranges and Cr/C ratios. The x-axis spans Cr/C values ranging from 1 to 15, reflecting the alloy compositions, while the y-axis represents deviation ranges, extending up to 30 %. Each deviation range, with a width of 2.5 %, is color-coded to indicate the corresponding count of alloys falling within that particular bin. For a given Cr/C value, the number of alloys falling within a certain deviation range using the various models can be observed. The intensity of the colour reflects the count of alloys within each bin, providing a visual representation of the model's predictive performance across different composition ranges.

A comparative analysis between the ML model and the M model, underscores the superior predictive performance of the ML model. Notably, the ML model demonstrates a more concentrated distribution of alloys within lower deviation ranges, indicative of its enhanced accuracy in predicting CVF values. For instance, at a Cr/C ratio of 6, the ML model displays a focal point of alloys with a deviation between 0 and 5 %, contrasting with the M model's broader dispersion across higher deviation ranges. This concentrated clustering towards lower deviations in the ML model suggests a more precise alignment between predicted and experimentally determined CVF values. The M model, in contrast, exhibits a more scattered distribution, particularly in the mid-range Cr/C ratios, implying a tendency for higher deviations in its predictions.

The heatmap representing the MNLR model, the second-best model after ML, reveals distinct patterns in comparison to the ML model. Notably, the MNLR model demonstrates competitive predictive capabilities, particularly evident in its concentration of alloys toward lower deviation ranges. At a Cr/C ratio of 6, akin to the ML model, the MNLR model exhibits a focal point of alloys with lower deviations, indicating a robust predictive alignment with experimentally determined CVF values. However, it's essential to note that while the ML model demonstrates a more consolidated clustering towards lower deviations, the MNLR model maintains a competitive performance with a dispersion across various Cr/C ratios.

Upon closer examination of the MNLR model at higher Cr/C ratios, particularly beyond a value of 10, a more dispersed distribution of alloy counts is observed across deviation ranges. In comparison to the ML

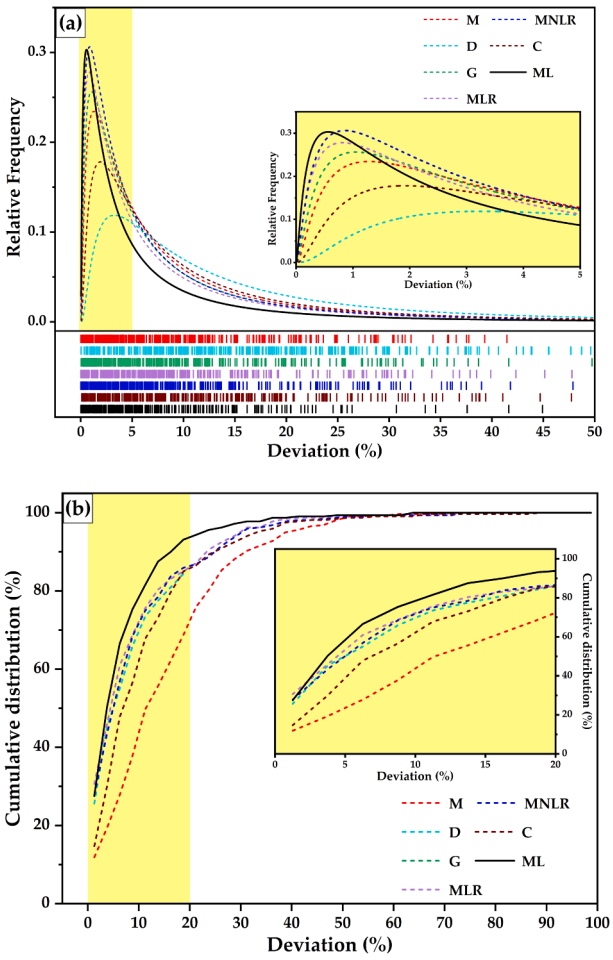

Fig. 5. (a) Distribution rug plot showing absolute deviation (%) against relative frequency for the ML model (solid black line) and other models (dotted lines). Inset focuses on deviations up to 5 %. (b) Cumulative distribution plot with inset (up to 20 %), comparing the percentage of alloys falling within deviation thresholds for ML and other models.

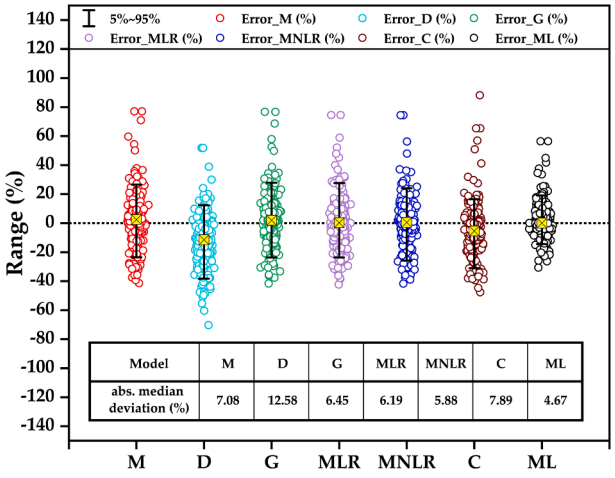

Model	M	D	G	MLR	MNLR	C	ML
abs. median deviation (%)	7.08	12.58	6.45	6.19	5.88	7.89	4.67

Fig. 6. Scatter box plot showing the deviations obtained for all alloys using the various models. Inset table indicates the absolute median deviation (%) for each model.

model, which maintains a concentrated clustering of alloys towards lower deviations even at higher Cr/C ratios, the MNLR model displays a broader distribution. This suggests that, while both models exhibit competitive performance, the ML model may demonstrate a slightly more robust predictive accuracy, especially in scenarios characterized by high Cr/C ratios. The MNLR model's tendency towards a wider distribution at higher ratios indicates a potential challenge in achieving precision in CVF predictions in alloys with richer chromium content. This analysis highlights the comparative strengths and considerations of the ML and MNLR models across varying composition ranges.

Table 5 presents a comprehensive overview of the alloy counts distributed across the distinct Cr/C ranges, with a specific emphasis on pinpointing the model exhibiting the least % absolute deviation in counts within each range. The various models are evaluated across three Cr/C ranges: 1.0–5.0, 5.1–10.0 and 10.1–15.0. Notably, the ML model emerges as the optimal performer, demonstrating the least percentage deviation in counts in all three ranges. Expanding on this analysis, when considering only the ML model across all three Cr/C ranges, the calculated absolute median deviation increases gradually from 3.92 % in the 1.0–5.0 Cr/C range to 4.6 % in the 5.1–10.0 Cr/C range and further to 6.54 % in the 10.1–15.0 Cr/C range. The observed trend indicates a gradual rise in median error with the widening Cr/C range, underscoring the necessity for a nuanced model evaluation and the importance of considering Cr/C range implications for prediction reliability.

3.3. CVF estimation challenges: Metallography and data compilation

Metallography, while a valuable technique for studying microstructures, exhibits limitations that impact the accuracy of estimating the CVF. The method is subject to potential inaccuracies due to sample preparation artifacts, manual counting errors, and inherent subjectivity

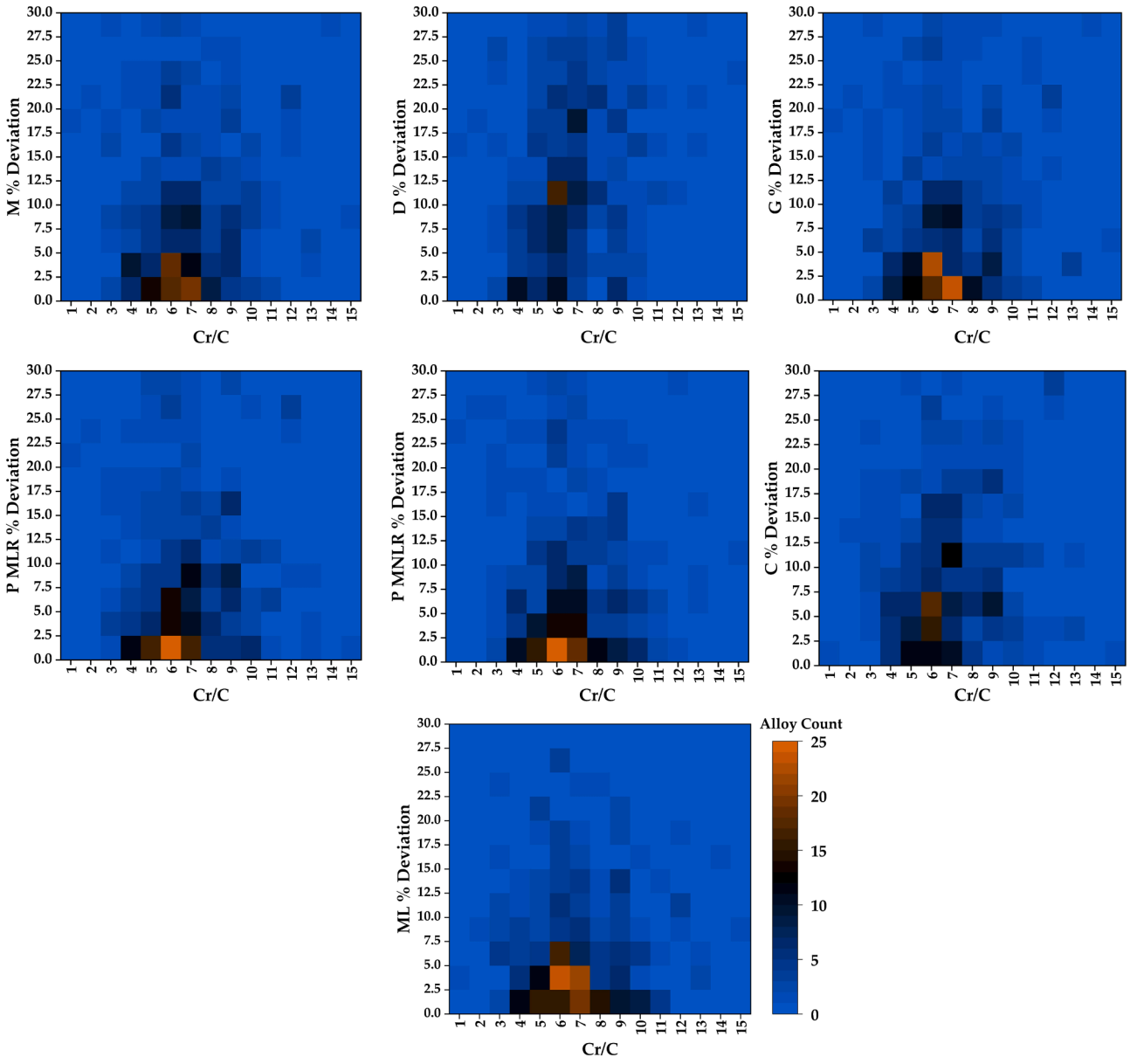

Fig. 7. Heatmap depicting the distribution of alloy counts across deviation ranges and Cr/C ratios.

Table 5
Comparative analysis of alloy counts and model performance across different Cr/C ranges.

Cr/C range	Total alloy count	Model with the least % deviation (counts)						
		M	D	G	MLR	MNLR	C	**ML**
1.0–5.0	66	7	10	1	7	7	12	**22**
5.1–10.0	228	28	32	16	29	36	26	**61**
10.1–15.0	23	4	1	1	5	4	1	**7**

in analysis [52–55]. The small sample size and limited representativeness of the chosen samples may compromise the statistical significance of the results. Additionally, variations in etching solutions, limited spatial resolution, and the influence of surface effects contribute to uncertainties in the observed microstructure [56–58].

Furthermore, collecting chemical composition data from diverse sources introduces challenges associated with data inconsistency, lack of standardization, and varying levels of data quality. The absence of standardized reporting formats and units across different manuscripts and theses can complicate the integration and comparison of information. Variability in measurement techniques and reporting methodologies adds another layer of complexity, impacting the harmonization of data. Addressing these issues requires meticulous attention to data cleaning, normalization, and documentation, as well as transparent reporting of any limitations in the dataset's reliability and generalizability. In general, it should be emphasized that valuable data is available in the literature, but the bottleneck for exploiting this data is the collection and preparation of the data. This once again highlights the need for FAIR (Findability, Accessibility, Interoperability, Reusability) data principles with accompanying, relevant metadata [59].

3.4. Outlook

In future advancements of CVF estimation models, there is an opportunity to refine predictions by accounting for the distinct influence of heat treatment on the alloy's microstructure. While the bulk chemical composition proves effective in forecasting CVF in the as-cast state, the introduction of heat treatment introduces a nuanced complexity. Unlike

eutectic carbides (EC) that tend to stay unaffected during heat treatment, it might be worthwhile to focus on the matrix composition as a key player in influencing the formation of secondary carbides (SC). The evolution of the alloy's microstructure, especially the precipitation of SC within the matrix, becomes a critical aspect to consider during heat treatment, the amount and distribution of which can lead to variation in the properties [11,20,60]. By fine-tuning the model to integrate both bulk and matrix compositions, it is anticipated that the predictive accuracy of CVF, particularly in the context of heat treatment-induced changes, can be significantly improved.

3.5. Data and model availability

The dataset as well as the trained ML model are available at https://doi.org/10.5281/zenodo.10654150 [47]. The repository includes the comprehensive dataset with all compositions and corresponding experimental CVF compiled from literature as well as the train and test splits used for training and evaluating the ML model. It also contains the final trained model and a MATLAB script for applying the model to calculate the CVF of new, unknown HCCI compositions. A list of all references that have been included in the dataset is also provided.

4. Conclusion

This study significantly broadened the scope of HCCI alloy compositions by encompassing a more extensive range of C and Cr content. Specifically, our dataset now spans alloys with carbon concentrations ranging from 1.38 wt% to 5.5 wt%, chromium concentrations ranging from 5 wt% to 37 wt%, and corresponding Cr/C ratios from 1 to 17. In comparison, Maratray's original model focused on a narrower range, with C concentrations from 1.95 wt% to 4.31 wt%, Cr concentrations from 10.8 wt% to 25.82 wt%, and Cr/C ratios from 3.5 to 10. This expansion allows for a comprehensive exploration of the predictive capabilities of our models within a broader spectrum of alloy compositions, capturing variations in Cr, C, and Cr/C ratios more thoroughly.

In conclusion, the implementation of ML techniques has brought forth a refined strategy for the estimation CVF in as-cast HCCI alloys. By leveraging ML algorithms and training models on a comprehensive dataset encompassing diverse alloy compositions, the accuracy of CVF estimation has been significantly improved across a broader spectrum of compositions. The influential role of C, Cr and Mo in determining CVF has been successfully identified, enabling more precise predictions. The ML-based methodology presented in this study provides a valuable tool that empowers researchers in the field to determine CVF in HCCI alloys without the need for laborious and resource-intensive experimental procedures.

CRediT authorship contribution statement

U. Pranav Nayak: Writing – original draft, Visualization, Investigation, Formal analysis, Data curation, Conceptualization. **Martin Müller:** Writing – original draft, Validation, Software, Formal analysis, Conceptualization. **Noah Quartz:** Data curation. **M. Agustina Guitar:** Funding acquisition, Supervision, Writing – review & editing. **Frank Mücklich:** Funding acquisition, Resources.

Declaration of competing interest

The authors declare that they have no known competing financial interests or personal relationships that could have appeared to influence the work reported in this paper.

Data availability

The dataset as well as the trained ML model are available at https://doi.org/10.5281/zenodo.10654150.

Acknowledgement

The present work is supported by funding from the Deutsche Forschungsgemeinschaft (DFG, project: GU 2102/2-1). Additionally, the EFRE Funds of the European Commission and the State Chancellery of Saarland for support of activities within the ZuMat project are acknowledged.

References

[1] G. Laird, R. Gundlach, K. Rohrig, Abrasion-resistant cast iron handbook, American Foundry Society, Schaumburg, Illinois (USA), 2000.
[2] ASM International, ASM Handbook Volume 15 - Casting, ASM International, Ohio, 2008, doi: 10.31399/asm.hb.v15.9781627081870.
[3] ASTM International, Standard Specification for Abrasion Resistance Cast Irons: ASTM Standard A 532/A 532M - 93a, West Conshohocken, PA, USA, 2003, www.astm.org.
[4] C.P. Tabrett, I.R. Sare, M.R. Ghomashchi, Microstructure-property relationships in high chromium white iron alloys, Int. Mater. Rev. 41 (1996) 59–82, https://doi.org/10.1179/095066096790326075.
[5] U.P. Nayak, Interplay between the microstructure and tribological performance in heat-treated high chromium cast iron alloys, PhD Thesis, Saarland University, 2023, doi: 10.22028/D291-40546.
[6] R.W. Durman, Progress in abrasion-resistant materials for use in comminution processes, Int. J. Miner. Process. 22 (1988) 381–399, https://doi.org/10.1016/0301-7516(88)90074-9.
[7] J. Dodd, Recent developments in abrasion resistant high chromium-molybdenum irons, low-alloy manganese steels and alloyed nodular irons of importance in the extraction and utilization of energy resources, J. Mater. Energy Syst. 2 (1980) 65–76, https://doi.org/10.1007/BF02833432.
[8] M.A. Guitar, S. Suárez, O. Prat, M. Duarte Guigou, V. Gari, G. Pereira, F. Mücklich, High chromium cast irons: destabilized-subcritical secondary carbide precipitation and its effect on hardness and wear properties, J. Mater. Eng. Perform. 27 (2018) 3877–3885, https://doi.org/10.1007/s11665-018-3347-1.
[9] A. Wiengmoon, Carbides in high chromium cast irons, Naresuan Univ. Eng. J. 6 (2011) 64–70, doi: 10.14456/nuej.2011.6.
[10] U.P. Nayak, S. Suárez, V. Pesnel, F. Mücklich, M.A. Guitar, Load dependent microstructural evolution in an as-cast 26% Cr high chromium cast iron during unlubricated sliding, Friction 10 (2022) 1258–1275, https://doi.org/10.1007/s40544-021-0553-x.
[11] U.P. Nayak, F. Mücklich, M.A. Guitar, Interplay between the microstructure and tribological performance of a destabilized 26 wt% Cr HCCI: the influence of temperature and heating rate, Tribol. Int. 185 (2023) 108532, https://doi.org/10.1016/j.triboint.2023.108532.
[12] E. Karantzalis, A. Lekatou, H. Mavros, Microstructure and properties of high chromium cast irons: effect of heat treatments and alloying additions, Int. J. Cast Met. Res. 22 (2009) 448–456, https://doi.org/10.1179/174313309X436637.
[13] H. Gasan, F. Erturk, Effects of a destabilization heat treatment on the microstructure and abrasive wear behavior of high-chromium white cast iron investigated using different characterization techniques, Metall. Mater. Trans. A 44 (2013) 4993–5005, https://doi.org/10.1007/s11661-013-1851-3.
[14] K.A. Kibble, J.T.H. Pearce, Influence of heat treatment on the microstructure and Hardness of 19% high-chromium cast irons, Cast Metals 6 (1993) 9–15, https://doi.org/10.1080/09534962.1993.11819121.
[15] A. Wiengmoon, T. Chairuangsri, J.T.H. Pearce, Effects of destabilisation heat treatment on microstructure, hardness and corrosion behaviour of 18wt.%Cr and 25wt.%Cr cast irons, Key Eng. Mater. 658 (2015) 76–80, https://doi.org/10.4028/www.scientific.net/KEM.658.76.
[16] A. Bedolla-Jacuinde, R. Correa, J.G. Quezada, C. Maldonado, Effect of titanium on the as-cast microstructure of a 16%chromium white iron, Mater. Sci. Eng. A 398 (2005) 297–308, https://doi.org/10.1016/j.msea.2005.03.072.
[17] B. Lu, J. Luo, S. Chiovelli, Corrosion and wear resistance of chrome white irons—a correlation to their composition and microstructure, Metall. Mater. Trans. A 37 (2006) 3029–3038, https://doi.org/10.1007/s11661-006-0184-x.
[18] J.K. Fulcher, T.H. Kosel, N.F. Fiore, The effect of carbide volume fraction on the low stress abrasion resistance of high Cr-Mo white cast irons, Wear 84 (1983) 313–325, https://doi.org/10.1016/0043-1648(83)90272-7.
[19] R.J. Llewellyn, S.K. Yick, K.F. Dolman, Scouring erosion resistance of metallic materials used in slurry pump service, Wear 256 (2004) 592–599, https://doi.org/10.1016/j.wear.2003.10.002.
[20] U.P. Nayak, F. Mücklich, M.A. Guitar, Time-dependant microstructural evolution and tribological behaviour of a 26 wt% Cr white cast iron subjected to a destabilization heat treatment, Met. Mater. Int. 29 (2023) 934–947, https://doi.org/10.1007/s12540-022-01276-8.
[21] K.H. Zum Gahr, G.T. Eldis, Abrasive wear of white cast irons, Wear 64 (1980) 175–194, https://doi.org/10.1016/0043-1648(80)90101-5.
[22] Ö.N. Doğan, J.A. Hawk, G. Laird, Solidification structure and abrasion resistance of high chromium white irons, Metall. Mater. Trans. A 28 (1997) 1315–1328, https://doi.org/10.1007/s11661-997-0267-3.
[23] C. He-Xing, C. Zhe-Chuan, L. Jin-Cai, L. Huai-Tao, Effect of niobium on wear resistance of 15%Cr white cast iron, Wear 166 (1993) 197–201, https://doi.org/10.1016/0043-1648(93)90262-K.

[24] I.R. Sare, B.K. Arnold, The influence of heat treatment on the high-stress abrasion resistance and fracture toughness of alloy white cast irons, Metall. Mater. Trans. A 26 (1995) 1785–1793, https://doi.org/10.1007/BF02670766.
[25] F. Maratray, R. Usseglio-Nanot, Atlas: transformation characteristics of chromium and chromium-molybdenum white irons, 1970, Country unknown/Code not available, 1970.
[26] F. Maratray, R. Usseglio-Nanot, Factors Affecting the Structure of Chromium and Chromium-Molybdenum White Irons, Climax Molybdenum S.A. Paris, Paris, 1971.
[27] M. Jokari-Sheshdeh, Y. Ali, S.C. Gallo, W. Lin, J.D. Gates, Effect of Cr: Fe ratio on the mechanical properties of (Cr, Fe)7C3 ternary carbides in abrasion-resistant white cast irons, J. Mater. Sci. 58 (2023) 7504–7521, https://doi.org/10.1007/s10853-023-08461-z.
[28] C. Le Nué, S. Corujeira Gallo, A. Vahid, J. Wang, M. Taherishargh, H. Attar, D. Fabijanic, M. Barnett, Destabilization treatment and its influence on microstructure and matrix Hardness of high-Cr cast iron, Metall. Mater. Trans. A 54 (2023) 4952–4965, https://doi.org/10.1007/s11661-023-07216-4.
[29] M. Jokari-Sheshdeh, Y. Ali, S.C. Gallo, W. Lin, J.D. Gates, Comparing the abrasion performance of NiHard-4 and high-Cr-Mo white cast irons: the effects of chemical composition and microstructure, Wear 492–493 (2022) 204208, https://doi.org/10.1016/j.wear.2021.204208.
[30] U.P. Nayak, M.A. Guitar, F. Mücklich, A comparative study on the influence of chromium on the phase fraction and elemental distribution in as-cast high chromium cast irons: simulation vs. experimentation, Metals (Basel) 10 (2020), https://doi.org/10.3390/met10010030.
[31] R.J. Chung, Comprehensive study of the abrasive wear and slurry erosion behavior of an expanded system of high chromium cast iron and microstructural modification for enhanced wear resistance, University of Alberta, 2014. PhD Thesis.
[32] J.W. Choi, S.K. Chang, Effects of molybdenum and copper additions on microstructure of high chromium cast iron rolls, ISIJ Int. 32 (1992) 1170–1176, https://doi.org/10.2355/isijinternational.32.1170.
[33] S. Imurai, C. Thanachayanont, J.T.H. Pearce, K. Tsuda, T. Chairuangsri, Effects of Mo on microstructure of as-cast 28 wt.% Cr-2.6 wt.% C-(0–10) wt.% Mo irons, Mater Charact 90 (2014) 99–112, https://doi.org/10.1016/j.matchar.2014.01.014.
[34] J. Gates, The challenge of accurate prediction of industrial wear performance from laboratory tests. International Symposium on Wear Resistant Alloys for the Mining and Processing Industry, Campinas, São Paulo, 2018.
[35] H. Pourasiabi, J.D. Gates, Effects of matrix chromium-to-carbon ratio on high-stress abrasive wear behavior of high chromium white cast irons dual-reinforced by niobium carbides, Tribol. Int. 167 (2022) 107350, https://doi.org/10.1016/j.triboint.2021.107350.
[36] F.S. Saleh, M.S. Aliakbarian, M. Salzmann, L. Petersson, J.M. Alvarez, Effective use of synthetic data for urban scene semantic segmentation, in: Lecture Notes in Computer Science (Including Subseries Lecture Notes in Artificial Intelligence and Lecture Notes in Bioinformatics), Springer, Cham, 2018, pp. 86–103, https://doi.org/10.1007/978-3-030-01216-8_6.
[37] O. Ronneberger, P. Fischer, T. Brox, U-net: convolutional networks for biomedical image segmentation BT - medical image computing and computer-assisted intervention – MICCAI 2015, Springer International Publishing, Cham, 2015, pp. 234–241.
[38] A. Mansouri Tehrani, A.O. Oliynyk, M. Parry, Z. Rizvi, S. Couper, F. Lin, L. Miyagi, T.D. Sparks, J. Brgoch, Machine learning directed search for ultraincompressible, superhard materials, J. Am. Chem. Soc. 140 (2018) 9844–9853, https://doi.org/10.1021/jacs.8b02717.
[39] E.A. Holm, R. Cohn, N. Gao, A.R. Kitahara, T.P. Matson, B. Lei, S.R. Yarasi, Overview: computer vision and machine learning for microstructural characterization and analysis, Metall. Mater. Trans. A 51 (2020) 5985–5999, https://doi.org/10.1007/s11661-020-06008-4.
[40] S.M. Azimi, D. Britz, M. Engstler, M. Fritz, F. Mücklich, Advanced steel microstructural classification by deep learning methods, Sci. Rep. 8 (2018) 1–14, https://doi.org/10.1038/s41598-018-20037-5.
[41] A.R. Durmaz, M. Müller, B. Lei, A. Thomas, D. Britz, E.A. Holm, C. Eberl, F. Mücklich, P. Gumbsch, A deep learning approach for complex microstructure inference, Nat. Commun. 12 (2021) 1–15, https://doi.org/10.1038/s41467-021-26565-5.
[42] W. Gang Li, L. Xie, Y. Zhao, Z. Li, W. Wang, Prediction model for mechanical properties of hot-rolled strips by deep learning, J. Iron Steel Res. Int. 27 (2020) 1045–1053, https://doi.org/10.1007/s42243-020-00450-9.
[43] Y.C. Hsu, C.H. Yu, M.J. Buehler, Using deep learning to predict fracture patterns in crystalline solids, Matter 3 (2020) 197–211, https://doi.org/10.1016/j.matt.2020.04.019.
[44] C. Shen, C. Wang, P.E.J. Rivera-Díaz-del-Castillo, D. Xu, Q. Zhang, C. Zhang, W. Xu, Discovery of marageing steels: machine learning vs. physical metallurgical modelling, J. Mater. Sci. Technol. 87 (2021) 258–268, https://doi.org/10.1016/j.jmst.2021.02.017.
[45] E.M. Askanazi, S. Yadav, I. Grinberg, Prediction of the Curie temperatures of ferroelectric solid solutions using machine learning methods, Comput. Mater. Sci. 199 (2021), https://doi.org/10.1016/j.commatsci.2021.110730.
[46] R. Tamura, G. Deffrennes, K. Han, T. Abe, H. Morito, Y. Nakamura, M. Naito, R. Katsube, Y. Nose, K. Terayama, Machine-Learning-based phase diagram construction for high-throughput batch experiments, Sci. Technol. Adv. Mater. Methods 2 (2022) 153–161, https://doi.org/10.1080/27660400.2022.2076548.
[47] M. Müller, U.P. Nayak, Carbide volume fraction estimation in as-cast HCCI alloys using, Mach. Learn. (2024), https://doi.org/10.5281/zenodo.10654150.
[48] A. Géron, Hands-on Machine Learning with Scikit-Learn, Keras & TensorFlow, O'Reilly Media, Inc., 2019.
[49] M. Ikeda, T. Umeda, C.P. Tong, T. Suzuki, N. Niwa, O. Kato, Effect of molybdenum addition on solidification structure, mechanical properties and wear resistivity of high chromium cast irons, ISIJ Int. 32 (1992) 1157–1162, https://doi.org/10.2355/isijinternational.32.1157.
[50] C. Scandian, C. Boher, J.D.B. de Mello, F. Rézaï-Aria, Effect of molybdenum and chromium contents in sliding wear of high-chromium white cast iron: the relationship between microstructure and wear, Wear 267 (2009) 401–408, https://doi.org/10.1016/j.wear.2008.12.095.
[51] A.R.H. Far, S.H.M. Anijdan, S.M. Abbasi, The effect of increasing Cu and Ni on a significant enhancement of mechanical properties of high strength low alloy, low carbon steels of HSLA-100 type, Mater. Sci. Eng. A 746 (2019) 384–393, https://doi.org/10.1016/j.msea.2019.01.025.
[52] J. Ohser, K. Sandau, W. Stets, W. Gerber, Bildanalytische Charakterisierung von Graphit im Grauguss und Klassifikation der Lamellenanordnung/Image Analytical Characterization of Graphite in Grey Cast Iron and Classification of Lamellar Arrangement, 40 (2003) 454–473, doi:10.1515/pm-2003-400906.
[53] J. Ohser, F. Mücklich, Statistical Analysis of Microstructures in Materials Science, first edition, Wiley, 2000.
[54] U.P. Nayak, M.A. Guitar, F. Mücklich, Evaluation of etching process parameter optimization in the objective specific microstructural characterization of as-cast and heat treated HCCI alloy, Pract. Metallogr. 57 (2020) 688–713, https://doi.org/10.3139/147.110682.
[55] U.P. Nayak, M. Müller, D. Britz, M.A. Guitar, F. Mücklich, Image processing using open source tools and their implementation in the analysis of complex microstructures, Pract. Metallogr. 58 (2021) 484–506, https://doi.org/10.1515/pm-2021-0039.
[56] ASM International, Metallography and Microstructures, ASM International, Ohio, USA, 2004, doi: 10.31399/asm.hb.v09.9781627081771.
[57] G.F. Vander Voort, Metallography: Principles and Practice, 1999.
[58] M.A. Guitar, A. Scheid, S. Suárez, D. Britz, M.D. Guigou, F. Mücklich, Secondary carbides in high chromium cast irons: an alternative approach to their morphological and spatial distribution characterization, Mater. Charact. 144 (2018) 621–630, https://doi.org/10.1016/j.matchar.2018.08.020.
[59] M.D. Wilkinson, M. Dumontier, I.J.J. Aalbersberg, G. Appleton, M. Axton, A. Baak, N. Blomberg, J.-W. Boiten, L.B. da Silva Santos, P.E. Bourne, J. Bouwman, A. J. Brookes, T. Clark, M. Crosas, I. Dillo, O. Dumon, S. Edmunds, C.T. Evelo, R. Finkers, A. Gonzalez-Beltran, A.J.G. Gray, P. Groth, C. Goble, J.S. Grethe, J. Heringa, P.A.C. 't Hoen, R. Hooft, T. Kuhn, R. Kok, J. Kok, S.J. Lusher, M. E. Martone, A. Mons, A.L. Packer, B. Persson, P. Rocca-Serra, M. Roos, R. van Schaik, S.-A. Sansone, E. Schultes, T. Sengstag, T. Slater, G. Strawn, M.A. Swertz, M. Thompson, J. van der Lei, E. van Mulligen, J. Velterop, A. Waagmeester, P. Wittenburg, K. Wolstencroft, J. Zhao, B. Mons, The FAIR guiding principles for scientific data management and stewardship, Sci. Data 3 (2016) 160018, https://doi.org/10.1038/sdata.2016.18.
[60] M.A. Guitar, U.P. Nayak, D. Britz, F. Mücklich, The effect of thermal processing and chemical composition on secondary carbide precipitation and hardness in high-chromium cast irons, Int. J. Met. 14 (2020) 755–765, https://doi.org/10.1007/s40962-020-00407-4.